Limit analysis of plates and slabs using a meshless equilibrium formulation

Canh V. Le, Matthew Gilbert* and Harm Askes

Department of Civil and Structural Engineering, The University of Sheffield, United Kingdom

SUMMARY

A meshless Element-Free Galerkin (EFG) equilibrium formulation is proposed to compute the limit loads which can be sustained by plates and slabs. In the formulation pure moment fields are approximated using a moving least squares technique, which means that the resulting fields are smooth over the entire problem domain. There is therefore no need to enforce continuity conditions at interfaces within the problem domain, which would be a key part of a comparable finite element formulation. The collocation method is used to enforce the strong form of the equilibrium equations and a stabilized conforming nodal integration scheme is introduced to eliminate numerical instability problems. The combination of the collocation method and the smoothing technique means that equilibrium only needs to be enforced at the nodes, and stable and accurate solutions can be obtained with minimal computational effort. The von Mises and Nielsen yield criteria which are used in the analysis of plates and slabs respectively are enforced by introducing second-order cone constraints, ensuring that the resulting optimization problem can be solved using efficient interior-point solvers. Finally, the efficacy of the procedure is demonstrated by applying it to various benchmark plate and slab problems.

KEY WORDS: Limit analysis; meshless methods; EFG; equilibrium model; second-order cone programming; plates; slabs.

1. INTRODUCTION

The fundamental theorems of limit analysis can be used to provide upper and lower bound estimates of the load required to cause collapse of a body or structure. If a suitable approximation for the displacement field is used, and the kinematic theorem is applied, an upper bound on the exact limit load can be obtained. Alternatively, if a suitable approximation for the stress field is used, and the static theorem is applied, a lower bound can be obtained. Applying these theorems and using a finite element discretization, numerical procedures have been developed to perform the limit analysis of perfectly plastic plates and slabs, e.g. [1–7]. These procedures can provide good bounds on the exact collapse load (or 'load multiplier'),

*Correspondence to: Matthew Gilbert, Department of Civil and Structural Engineering, University of Sheffield, Sheffield, S1 3JD, United Kingdom, e-mail: m.gilbert@sheffield.ac.uk

with the results in [1] remarkably providing the best lower-bounds available for plate problems for many years [8]. However, finite element based computational limit analysis methods have drawbacks, and have to date not found widespread use in engineering practice. It is therefore desirable to explore a range alternative methods. Recently Le et al. [9] proposed a numerical kinematic formulation using the Element-Free Galerkin (EFG) method and second-order cone programming (SOCP) to furnish good (approximate) upper-bound solutions for Kirchhoff plate problems governed by the von Mises failure criterion. It has also been demonstrated [9, 10] that the EFG method is in general well suited for limit analysis problems, allowing accurate solutions to be obtained with relatively few nodes. Following this line of research, the main objective of this paper is to develop an equilibrium formulation which combines the EFG method with SOCP to obtain accurate solutions for both plate and slab problems.

In a static equilibrium formulation, the stress/moment fields are generally chosen so that the equilibrium equations, boundary conditions and continuity requirements are met for all feasible values of the problem variables. In Chen et al. [10], a self-equilibrium stress basis vector at each Gaussian point is calculated by solving the equivalent weak form of the equilibrium equations. The self-equilibrium stress field is then obtained by a linear combination of several self-equilibrium stress basis vectors which are generated by considering the differences between intermediate stresses during the elasto-plastic equilibrium iteration. However, the stress field obtained is not guaranteed to be statically admissible as it is derived from an approximated virtual displacement field by solving the weak form of the equilibrium equation. In contrast, in this paper the stress/moment fields will be constructed by using a moving least squares approximation. It is well-known that the field obtained when using this technique is smooth over the entire problem domain. There is therefore no need to enforce continuity conditions at interfaces within the problem domain (which would be a key part of a comparable finite element formulation).

In the framework of meshfree methods, it is advantageous if the problem under consideration can be solved be evaluating quantities at the nodes only. For problems involving integration, a stabilized conforming nodal integration (SCNI) scheme proposed in [11] is an effective option. The main idea of the scheme is that nodal values are determined by spatially averaging field values using the divergence theorem. The scheme has been applied successfully to various analysis problems [9, 12–14]. It is shown that, when the SCNI scheme is applied, the solutions obtained are accurate and stable, and the computational cost is much lower than when using Gauss integration. Due to these advantages the scheme will be used here to stabilize the moment derivatives. Using smoothed second derivatives of the moment field at nodes, the equilibrium equations only need to be fulfilled at the nodes. Furthermore, properties of Voronoi cells (which are representative nodal domains used in the smoothing scheme) can be used as a reference when enforcing the yield criteria.

The aim of this paper is to present an EFG based equilibrium limit analysis formulation for application to rigid-perfectly plastic plates and slabs, governed by the von Mises and Nielsen yield criteria respectively. The Kirchhoff moment field is approximated by using the moving least squares technique and nodal collocation is used to impose boundary conditions. The yield criteria are cast in terms of conic constraints, allowing the limit analysis problem to be posed as a standard second-order cone programming problem which can be solved using highly efficient solvers [15]. Finally, in order to test the performance of the method, several benchmark plate and slab examples from the literature are investigated.

2. LIMIT ANALYSIS OF PLATES - EQUILIBRIUM FORMULATION

A lower-bound solution to the problem involving a rigid-perfectly plastic plate or slab can be obtained by using the static theorem of plasticity, which states that a moment field is statically and plastically admissible if (i) equilibrium and boundary conditions are fully satisfied, and (ii) the yield condition is not violated anywhere. The exact plastic collapse load multiplier, λ_p, is the largest value among a set of lower bound multipliers, λ^-, corresponding to any statically and plastically admissible moment distribution [1, 4]. The moment field is denoted as $\mathbf{m} = [m_{xx}\ m_{yy}\ m_{xy}]^T$ and is constrained to belong to the domain

$$\mathcal{B} = \{\mathbf{m} \,|\, \psi(\mathbf{m}) \leq 0\}\,, \tag{1}$$

in which the so-called yield function $\psi(\mathbf{m})$ is convex.

In this study, the yield criterion proposed by Nielsen [16–18] is used for the analysis of reinforced concrete slabs. The criterion is expressed as

$$\begin{aligned} (m^+_{px} - m_{xx})(m^+_{py} - m_{yy}) &\geq m^2_{xy} \\ (m^-_{px} + m_{xx})(m^-_{py} + m_{yy}) &\geq m^2_{xy} \\ -m^-_{px} \leq m_{xx} &\leq m^+_{px} \\ -m^-_{py} \leq m_{yy} &\leq m^+_{py} \end{aligned} \tag{2}$$

where m^-_{px} and m^-_{py} are the negative yield moments in the x and y directions, respectively, and similarly m^+_{px} and m^+_{py} are the positive yield moments in the two directions. The constraints in (2) represent a bi-conical yield surface, as shown in Figure 1.

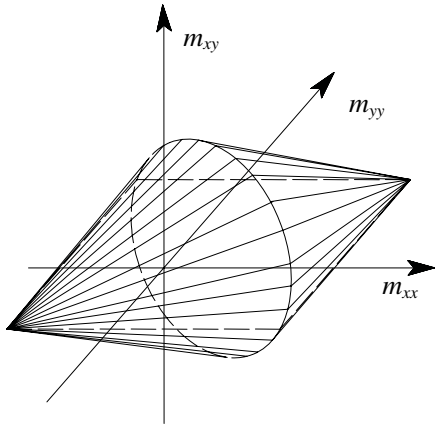

Figure 1. Yield criterion for reinforced concrete slabs (after Nielsen [16–18])

For steel plates, the von Mises failure criterion is often used, and can be expressed as

$$\psi(\mathbf{m}) = \sqrt{\mathbf{m}^T\ \mathbf{P}\ \mathbf{m}} - m_p \tag{3}$$

where $m_p = \sigma_0 t^2/4$ is the plastic moment of resistance per unit width of a plate of thickness

t and yield stress σ_0, and where

$$\mathbf{P} = \frac{1}{2}\begin{bmatrix} 2 & -1 & 0 \\ -1 & 2 & 0 \\ 0 & 0 & 6 \end{bmatrix} \tag{4}$$

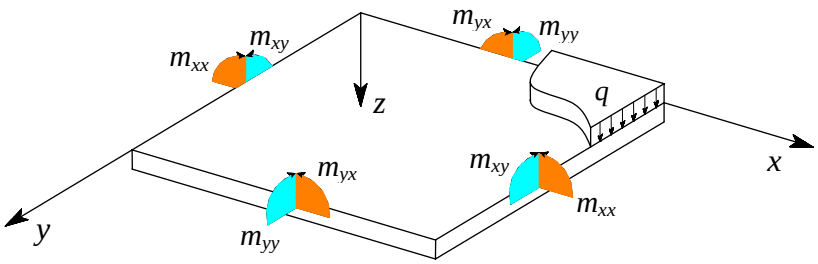

Figure 2. Plate sign conventions

Following the sign convention given in Figure 2, the lower-bound limit analysis of plate/slab problems can be expressed in the form of a mathematical programming problem, as

$$\lambda^- = \max\ \lambda \tag{5a}$$

$$\text{s.t}\quad \nabla^2\mathbf{m} + \lambda q = 0 \tag{5b}$$

$$\mathbf{m} \in \mathcal{B} \tag{5c}$$

where λ^- is the numerically computed load multiplier, q is the pressure load, $\nabla^2 = \left\{ \frac{\partial^2}{\partial x^2} \quad \frac{\partial^2}{\partial y^2} \quad 2\frac{\partial^2}{\partial x \partial y} \right\}$, and the moment field $\mathbf{m}$ must also satisfy appropriate boundary conditions.

3. THE EFG EQUILIBRIUM MODEL

3.1. Moving least squares approximation

Whereas in the kinematic formulation the displacement field is approximated, here the moment field needs to be approximated. By using the moving least squares technique [19], which is the most frequently used approximation in meshless methods, approximations of these moment fields can be expressed as

$$\mathbf{m}^h(\mathbf{x}) = \begin{bmatrix} m^h_{xx} \\ m^h_{yy} \\ m^h_{xy} \end{bmatrix} = \sum_{I=1}^{n} \Phi_I(\mathbf{x}) \begin{bmatrix} m_{xxI} \\ m_{yyI} \\ m_{xyI} \end{bmatrix} \tag{6}$$

in which

$$\Phi_I(\mathbf{x}) = \mathbf{p}^T(\mathbf{x})\mathbf{A}^{-1}(\mathbf{x})\mathbf{B}_I(\mathbf{x}) \tag{7}$$

$$\mathbf{A}(\mathbf{x}) = \sum_{I=1}^{n} w_I(\mathbf{x})\mathbf{p}^T(\mathbf{x}_I)\mathbf{p}(\mathbf{x}_I) \tag{8}$$

$$\mathbf{B}_I(\mathbf{x}) = w_I(\mathbf{x})\mathbf{p}(\mathbf{x}_I) \tag{9}$$

where n is the number of nodes; $\mathbf{p}(\mathbf{x})$ is a set of basis functions; $w_I(\mathbf{x})$ is a weight function associated with node I. In this work, an isotropic quartic spline function is used, which is given by

$$w_I(\mathbf{x}) = \begin{cases} 1 - 6s^2 + 8s^3 - 3s^4 & \text{if } s \leq 1 \\ 0 & \text{if } s > 1 \end{cases} \tag{10}$$

with $s = \frac{\|\mathbf{x}-\mathbf{x}_I\|}{R_I}$, where R_I is the support radius of node I and determined by

$$R_I = \beta \cdot h_I \tag{11}$$

where β is the dimensionless size of influence domain and h_I is the nodal spacing when nodes were distributed regularly, or the maximum distance to neighbouring nodes when nodes were distributed irregularly (Figure 3). The maximum distance is determined by

$$h_I = \max\{d_J : d_J = \overline{P_I P_J},\ \forall P_J \in N_I\} \tag{12}$$

where

$$\begin{aligned} N_I &= \{P_J : V(P_J) \cap V(P_I) \neq \oslash\} \\ &= \{p_1, p_2, p_3, p_4, p_5, p_6, p_7\} \end{aligned} \tag{13}$$

in which $V(P_I)$ is the Voronoi cell of particle P_I.

3.2. Stabilized equilibrium equation

The equilibrium equations are frequently treated in one of two ways in numerical procedures: (i) equilibrium is enforced at nodes in the problem domain and also at boundaries (using the 'collocation' method), or (ii) the equilibrium equations are transformed into the equivalent weak-form (involving integrals), using the so-called 'weighted residual method' [20, 21]. The former method is simple and fast, but it has been reported to suffer from numerical stability problems [21, 22]. In contrast, formulations which use the weak-form can usually produce a stable set of discretized system equations, in turn leading to accurate solutions. Finite element based formulations have been developed by several authors [23, 24]. Considering meshless methods, an equilibrium model for elastostatic problems was first introduced in [25], where stress fields were expressed by means of an Airy stress function, approximated using the moving least squares method. Alternatively the self-equilibrium stress field can be calculated by using an assumed displacement field and solving the weak form of the equilibrium equations [10]. However, here an alternative EFG equilibrium formulation in which the collocation method is used in combination with a smoothing technique is proposed.

A strain smoothing method was firstly presented in [26] for the regularization of material instabilities. The strain smoothing method was then modified to allow stabilization in nodal integration schemes, leading to the so-called stabilized conforming nodal integration (SCNI) scheme [11]. The SCNI scheme was then successfully applied to both elastic analysis [12, 13] and plastic analysis [9] problems. It has been shown that the SCNI scheme results in an efficient and truly mesh-free method, and also to numerically stable solutions. This smoothing technique will now be adapted in order to stabilize problems involving bending moment derivatives as follows

$$\tilde{m}^h_{,\alpha\beta}(\mathbf{x}_j) = \int_{\Omega_j} m^h_{,\alpha\beta}(\mathbf{x})\varphi(\mathbf{x}, \mathbf{x} - \mathbf{x}_j)\, \mathrm{d}\Omega \tag{14}$$

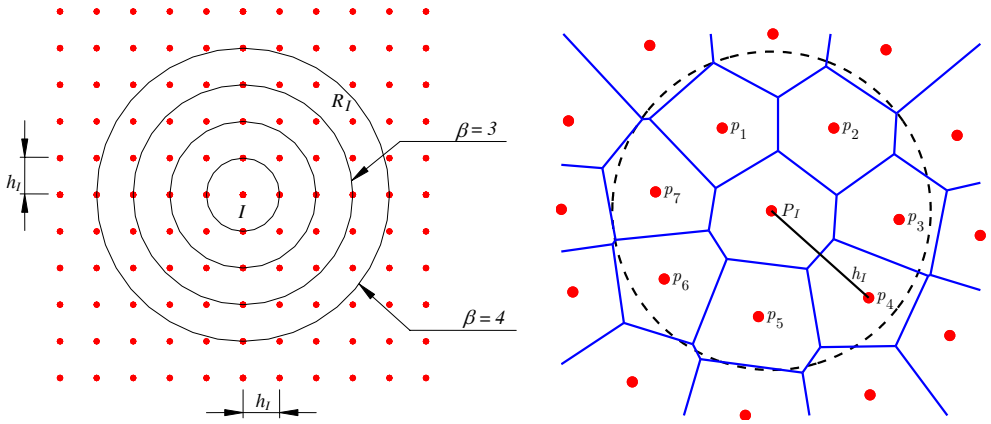

(a) Regular nodal layout (b) Irregular nodal layout

Figure 3. Sizes of influence domain

where $\tilde{m}^h_{,\alpha\beta}$ is the smoothed value of the second-derivative of moment $m^h_{,\alpha\beta}$ at node j, and φ is a distribution (or 'smoothing') function that has to satisfy the following properties [14, 26]

$$\varphi \geq 0 \quad \text{and} \quad \int_{\Omega_j} \varphi \, \mathrm{d}\Omega = 1 \tag{15}$$

For simplicity, the function φ is assumed to be a piecewise constant function and is given by

$$\varphi(\mathbf{x}, \mathbf{x} - \mathbf{x}_j) = \begin{cases} 1/a_j, & \mathbf{x} \in \Omega_j \\ 0, & \mathbf{x} \notin \Omega_j \end{cases} \tag{16}$$

where a_j is the area of the representative domain of node j, as shown in Figure 4.

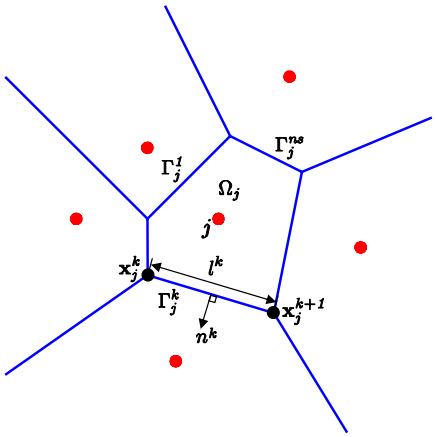

Figure 4. Geometry of a representative nodal domain

Substituting Equation (16) into Equation (14), and applying the divergence theorem, the following expressions can be derived

$$\begin{aligned} \tilde{m}^h_{,\alpha\beta}(\mathbf{x}_j) &= \frac{1}{a_j}\int_{\Omega_j} m^h_{,\alpha\beta}(\mathbf{x})\,\mathrm{d}\Omega \\ &= \frac{1}{2a_j}\int_{\Gamma_j}\left(m^h_{,\alpha}(\mathbf{x})n_\beta(\mathbf{x}) + m^h_{,\beta}(\mathbf{x})n_\alpha(\mathbf{x})\right)\,\mathrm{d}\Gamma \end{aligned} \tag{17}$$

where Γ_j is the boundary of the representative domain Ω_j.

Now introducing a moving least squares approximation of the moment fields, the smooth version of the moment second-derivative can be expressed as

$$\tilde{m}^h_{,\alpha\beta}(\mathbf{x}_j) = \sum_{I=1}^{n} \tilde{\Phi}_{I,\alpha\beta}(\mathbf{x}_j) m_{\alpha\beta I} \tag{18}$$

with

$$\begin{aligned} \tilde{\Phi}_{I,\alpha\beta}(\mathbf{x}_j) &= \frac{1}{2a_j}\int_{\Gamma_j}\left(\Phi_{I,\alpha}(\mathbf{x}_j)n_\beta(\mathbf{x}) + \Phi_{I,\beta}(\mathbf{x}_j)n_\alpha(\mathbf{x})\right)\mathrm{d}\Gamma \\ &= \frac{1}{4a_j}\sum_{k=1}^{ns}\left(n^k_\beta\, l^k + n^{k+1}_\beta\, l^{k+1}\right)\Phi_{I,\alpha}(\mathbf{x}^{k+1}_j) \\ &+ \frac{1}{4a_j}\sum_{k=1}^{ns}\left(n^k_\alpha\, l^k + n^{k+1}_\alpha\, l^{k+1}\right)\Phi_{I,\beta}(\mathbf{x}^{k+1}_j) \end{aligned} \tag{19}$$

where $\tilde{\Phi}$ is the smoothed version of Φ; ns is the number of segments of a Voronoi nodal domain Ω_j as shown in the Figure 4; $\mathbf{x}^k_j$ and $\mathbf{x}^{k+1}_j$ are the coordinates of the two end points of boundary segment Γ^k_j which has length l^k and outward surface normal n^k.

With the use of the smoothed value $\tilde{m}^h_{,\alpha\beta}$ the equilibrium equation can be enforced at n nodes, and Equation (5b) can be rewritten as

$$\mathbf{A}_1\mathbf{m}_1 + \mathbf{A}_2\mathbf{m}_2 + \mathbf{A}_3\mathbf{m}_3 + \lambda q\mathbf{I} = \mathbf{0} \tag{20}$$

where $\mathbf{I}$ is a $n \times n$ identity matrix, and

$$\mathbf{A}_1 = \begin{bmatrix} \cdots & \cdots & \cdots & \cdots \\ \tilde{\Phi}_{1,xx}(\mathbf{x}_j) & \tilde{\Phi}_{2,xx}(\mathbf{x}_j) & \cdots & \tilde{\Phi}_{n,xx}(\mathbf{x}_j) \\ \cdots & \cdots & \cdots & \cdots \end{bmatrix}_{n\times n} \tag{21}$$

$$\mathbf{A}_2 = \begin{bmatrix} \cdots & \cdots & \cdots & \cdots \\ \tilde{\Phi}_{1,yy}(\mathbf{x}_j) & \tilde{\Phi}_{2,yy}(\mathbf{x}_j) & \cdots & \tilde{\Phi}_{n,yy}(\mathbf{x}_j) \\ \cdots & \cdots & \cdots & \cdots \end{bmatrix}_{n\times n} \tag{22}$$

$$\mathbf{A}_3 = \begin{bmatrix} \cdots & \cdots & \cdots & \cdots \\ 2\tilde{\Phi}_{1,xy}(\mathbf{x}_j) & 2\tilde{\Phi}_{2,xy}(\mathbf{x}_j) & \cdots & 2\tilde{\Phi}_{n,xy}(\mathbf{x}_j) \\ \cdots & \cdots & \cdots & \cdots \end{bmatrix}_{n\times n} \tag{23}$$

$$\mathbf{m}_1 = \begin{bmatrix} m_{xx1} & \cdots & m_{xxn} \end{bmatrix}^T \tag{24}$$

$$\mathbf{m}_2 = \left[\begin{array}{ccc} m_{yy1} & \dots & m_{yyn} \end{array} \right]^T \tag{25}$$

$$\mathbf{m}_3 = \left[\begin{array}{ccc} m_{xy1} & \dots & m_{xyn} \end{array} \right]^T \tag{26}$$

It is important to note that when the smoothing technique is used, the equilibrium equation is fulfilled at nodes only (unlike in [10] where the equilibrium is transformed into the equivalent weak form and enforced at Gauss points).

3.3. Enforcement of boundary conditions

It should be borne in mind that the quantities m_{xxI}, m_{yyI} and m_{xyI} in Equation (6) are fictitious nodal values, rather than actual moments acting at the nodes. This unfortunately complicates matters when seeking to enforce boundary conditions. One way of addressing this is to use the collocation method proposed in [27]. Let M_n, M_{nt} and Q_n denote the normal bending moment, twisting moment and transverse shear force at node $\mathbf{x}_b$ on a free unloaded edge, where its normal vector $\mathbf{n}$ forms an angle α with the x-axis. Conditions for this boundary can be expressed as

$$\begin{array}{rcl} M_n & \equiv & m^h_{xx} c^2_\alpha + m^h_{yy} s^2_\alpha + 2 m^h_{xy} c_\alpha s_\alpha = 0 \\ M_{nt} & \equiv & (m^h_{yy} - m^h_{xx}) c_\alpha s_\alpha + 2 m^h_{xy} (c^2_\alpha - s^2_\alpha) = 0 \\ Q_n & \equiv & Q_x c_\alpha + Q_y s_\alpha = 0 \end{array} \tag{27}$$

where $c_\alpha = \cos\alpha$ and $s_\alpha = \sin\alpha$. It is important to note that smoothed moment derivatives are used in the equilibrium equation (20). Consequently, the shear forces Q_x and Q_y must also be calculated from these smoothed moment derivatives as follows

$$Q_x = \frac{\partial \tilde{m}_{xx}}{\partial x} + \frac{\partial \tilde{m}_{xy}}{\partial y} \tag{28}$$

$$Q_y = \frac{\partial \tilde{m}_{xy}}{\partial x} + \frac{\partial \tilde{m}_{yy}}{\partial y} \tag{29}$$

Introducing a moving least squares approximation of the moment field, Equation (27) can be rewritten as

$$\mathbf{B}_1 \mathbf{m}_1 + \mathbf{B}_2 \mathbf{m}_2 + \mathbf{B}_3 \mathbf{m}_3 = \mathbf{0} \tag{30}$$

where

$$\mathbf{B}_1 = \left[\begin{array}{cccc} \dots & \dots & \dots & \dots \\ c^2_\alpha \Phi_1(\mathbf{x}_i) & c^2_\alpha \Phi_2(\mathbf{x}_i) & \dots & c^2_\alpha \Phi_n(\mathbf{x}_i) \\ \dots & \dots & \dots & \dots \\ -c_\alpha s_\alpha \Phi_1(\mathbf{x}_i) & -c_\alpha s_\alpha \Phi_2(\mathbf{x}_i) & \dots & -c_\alpha s_\alpha \Phi_n(\mathbf{x}_i) \\ \dots & \dots & \dots & \dots \\ c_\alpha \tilde{\Phi}_{1,x}(\mathbf{x}_i) & c_\alpha \tilde{\Phi}_{2,x}(\mathbf{x}_i) & \dots & c_\alpha \tilde{\Phi}_{n,x}(\mathbf{x}_i) \\ \dots & \dots & \dots & \dots \end{array} \right] \tag{31}$$

$$\mathbf{B}_2 = \begin{bmatrix} \cdots & \cdots & \cdots & \cdots \\ s_\alpha^2\Phi_1(\mathbf{x}_i) & s_\alpha^2\Phi_2(\mathbf{x}_i) & \cdots & s_\alpha^2\Phi_n(\mathbf{x}_i) \\ \cdots & \cdots & \cdots & \cdots \\ c_\alpha s_\alpha\Phi_1(\mathbf{x}_i) & c_\alpha s_\alpha\Phi_2(\mathbf{x}_i) & \cdots & c_\alpha s_\alpha\Phi_n(\mathbf{x}_i) \\ \cdots & \cdots & \cdots & \cdots \\ s_\alpha\tilde{\Phi}_{1,y}(\mathbf{x}_i) & s_\alpha\tilde{\Phi}_{2,y}(\mathbf{x}_i) & \cdots & s_\alpha\tilde{\Phi}_{n,y}(\mathbf{x}_i) \\ \cdots & \cdots & \cdots & \cdots \end{bmatrix} \tag{32}$$

$$\mathbf{B}_3 = \begin{bmatrix} \cdots & \cdots & \cdots & \cdots \\ 2c_\alpha s_\alpha\Phi_1(\mathbf{x}_i) & 2c_\alpha s_\alpha\Phi_2(\mathbf{x}_i) & \cdots & 2c_\alpha s_\alpha\Phi_n(\mathbf{x}_i) \\ \cdots & \cdots & \cdots & \cdots \\ 2(c_\alpha^2 - s_\alpha^2)\Phi_1(\mathbf{x}_i) & 2(c_\alpha^2 - s_\alpha^2)\Phi_2(\mathbf{x}_i) & \cdots & 2(c_\alpha^2 - s_\alpha^2)\Phi_n(\mathbf{x}_i) \\ \cdots & \cdots & \cdots & \cdots \\ |s_\alpha\tilde{\Phi}_{1,x} + c_\alpha\tilde{\Phi}_{1,y}|_{\mathbf{x}_i} & |s_\alpha\tilde{\Phi}_{1,x} + c_\alpha\tilde{\Phi}_{2,y}|_{\mathbf{x}_i} & \cdots & |s_\alpha\tilde{\Phi}_{1,x} + c_\alpha\tilde{\Phi}_{n,y}|_{\mathbf{x}_i} \\ \cdots & \cdots & \cdots & \cdots \end{bmatrix} \tag{33}$$

where $i = 1, 2, \ldots, n_b$, and where n_b is the number of nodes with boundary conditions.

4. SECOND-ORDER CONE PROGRAMMING (SOCP)

It was recognized in [28] that most commonly used yield criteria can be cast in the form of conic constraints, and optimization problems involving such constraints can be solved using highly efficient solvers [15]. Consequently, several numerical limit analysis procedures which involve the use of cone programming techniques have been reported recently [9, 29, 30]. This paper continues this trend by combining SOCP with the presented EFG equilibrium model.

There are two types of second-order cone (also known as 'Lorentz' or 'ice cream' cones) in general use. The first is the standard quadratic cone, defined as

$$\mathscr{L}_q = \left\{ \boldsymbol{x} \in \mathbb{R}^m \mid x_1 \geq \sqrt{\sum_{j=2}^{m} x_j^2} = \|\boldsymbol{x}_{2\to m}\|_{L^2} \right\} \tag{34}$$

and the second is the rotated quadratic cone, defined as

$$\mathscr{L}_r = \left\{ \mathbf{x} \in \mathbb{R}^{m+2} \mid x_1 x_2 \geq \sum_{j=3}^{m+2} x_j^2 = \|\mathbf{x}_{3\to m+2}\|_{L^2}^2,\ x_1,\, x_2 \geq 0 \right\} \tag{35}$$

In the following sections, the Nielsen and von Mises yield criteria will be formulated using rotated and standard quadratic cones respectively.

4.1. The Nielsen yield criterion

Introducing additional problem variables as follows

$$\boldsymbol{\rho}^+ = \begin{bmatrix} \rho_1^+ \\ \rho_2^+ \\ \rho_3^+ \end{bmatrix} = \begin{bmatrix} m_{px}^+ - m_{xx}^h \\ m_{py}^+ - m_{yy}^h \\ \sqrt{2}\, m_{xy}^h \end{bmatrix} = \mathbf{D}^+\mathbf{m} + \mathbf{d}^+ \tag{36}$$

$$\boldsymbol{\rho}^- = \begin{bmatrix} \rho_1^- \\ \rho_2^- \\ \rho_3^- \end{bmatrix} = \begin{bmatrix} m_{px}^- + m_{xx}^h \\ m_{py}^- + m_{yy}^h \\ \sqrt{2}\, m_{xy}^h \end{bmatrix} = \mathbf{D}^- \mathbf{m} + \mathbf{d}^- \tag{37}$$

where

$$\mathbf{D}^+ = \begin{bmatrix} -1 & 0 & 0 \\ 0 & -1 & 0 \\ 0 & 0 & \sqrt{2} \end{bmatrix};\ \mathbf{d}^+ = \begin{bmatrix} m_{px}^+ \\ m_{py}^+ \\ 0 \end{bmatrix};\ \mathbf{D}^- = \begin{bmatrix} 1 & 0 & 0 \\ 0 & 1 & 0 \\ 0 & 0 & \sqrt{2} \end{bmatrix};\ \mathbf{d}^- = \begin{bmatrix} m_{px}^- \\ m_{py}^- \\ 0 \end{bmatrix} \tag{38}$$

the relations in Equation (2) are the intersection of two rotated cones and are expressed as

$$\boldsymbol{\rho}^+ \in \mathscr{L}_r^+,\ \ \mathscr{L}_r^+ = \left\{ \boldsymbol{\rho}^+ \in \mathbb{R}^3 \mid 2\rho_1^+ \rho_2^+ \geq (\rho_3^+)^2,\ \rho_1^+,\ \rho_2^+ \geq 0 \right\} \tag{39}$$

$$\boldsymbol{\rho}^- \in \mathscr{L}_r^-,\ \ \mathscr{L}_r^- = \left\{ \boldsymbol{\rho}^- \in \mathbb{R}^3 \mid 2\rho_1^- \rho_2^- \geq (\rho_3^-)^2,\ \rho_1^-,\ \rho_2^- \geq 0 \right\} \tag{40}$$

4.2. The von Mises yield criterion

In order to represent the von Mises criterion as a second-order cone constraint, Equation (41) is first rewritten in terms of the L^2 norm as

$$\psi(\mathbf{m}) = \|\mathbf{J}^T\, \mathbf{m}\|_{L^2} - m_p \tag{41}$$

where $\mathbf{J}$ is the so-called Cholesky factor of $\mathbf{P}$

$$\mathbf{J} = \frac{1}{2} \begin{bmatrix} 2 & 0 & 0 \\ -1 & \sqrt{3} & 0 \\ 0 & 0 & 2\sqrt{3} \end{bmatrix} \tag{42}$$

By applying the following transformation of the moment variables $\mathbf{m}$

$$\boldsymbol{\rho}_{2\to 4} = \begin{bmatrix} \rho_2 \\ \rho_3 \\ \rho_4 \end{bmatrix} = \mathbf{J}^T\, \mathbf{m} = \begin{bmatrix} m_{xx}^h - \dfrac{1}{2}\, m_{yy}^h \\ \dfrac{\sqrt{3}}{2}\, m_{yy}^h \\ \sqrt{3}\, m_{xy}^h \end{bmatrix} \tag{43}$$

and defining $\rho_1 = m_p$, constraint (1) can be cast in terms of a second-order cone constraint as follows

$$\mathcal{B} \equiv \mathscr{L}_q = \left\{ \boldsymbol{\rho} \in \mathbb{R}^4 \mid \rho_1 \geq \|\boldsymbol{\rho}_{2\to 4}\|_{L^2} = \sqrt{\rho_2^2 + \rho_3^2 + \rho_4^2},\ \rho_1 = m_p \right\} \tag{44}$$

where $\mathscr{L}_q$ is the four-dimensional quadratic cone and $\boldsymbol{\rho}^T = \{\rho_1\ \rho_2\ \rho_3\ \rho_4\}$.

Using a moving least squares approximation of the moment fields, the vector $\boldsymbol{\rho}_{2\to 4}$ is evaluated at point $\mathbf{x}_k$ and expressed as

$$\boldsymbol{\rho}_{2\to 4}^k = \mathbf{C}_k \mathbf{M} \tag{45}$$

where $\mathbf{M} = [\ \mathbf{m}_1\ \ \mathbf{m}_2\ \ \mathbf{m}_3\ ]^T$ and

$$\mathbf{C}_k = \begin{bmatrix} \mathbf{C}_{1k}^T & -\frac{1}{2}\,\mathbf{C}_{2k}^T & \mathbf{0} \\ \mathbf{0} & \frac{\sqrt{3}}{2}\,\mathbf{C}_{2k}^T & \mathbf{0} \\ \mathbf{0} & \mathbf{0} & \sqrt{3}\,\mathbf{C}_{3k}^T \end{bmatrix} \tag{46}$$

with

$$\begin{aligned} \mathbf{C}_{1k}^T &= \begin{bmatrix} \Phi_{1,xx}(\mathbf{x}_k) & \Phi_{2,xx}(\mathbf{x}_k) & \dots & \Phi_{n,xx}(\mathbf{x}_k) \end{bmatrix} \\ \mathbf{C}_{2k}^T &= \begin{bmatrix} \Phi_{1,yy}(\mathbf{x}_k) & \Phi_{2,yy}(\mathbf{x}_k) & \dots & \Phi_{n,yy}(\mathbf{x}_k) \end{bmatrix} \\ \mathbf{C}_{3k}^T &= \begin{bmatrix} \Phi_{1,xy}(\mathbf{x}_k) & \Phi_{2,xy}(\mathbf{x}_k) & \dots & \Phi_{n,xy}(\mathbf{x}_k) \end{bmatrix} \end{aligned} \tag{47}$$

Consequently, the quadratic cone at point $\mathbf{x}_k$ is

$$\mathscr{L}_q^k = \left\{ \boldsymbol{\rho}^k \in \mathbb{R}^4 \mid \rho_1 \geq \|\boldsymbol{\rho}_{2\to 4}^k\|_{L^2},\ \rho_1 = m_p \right\} \tag{48}$$

4.3. Limit analysis formulation

The limit analysis formulation can now be expressed in the form of a standard second-order cone programming problem as

$$\begin{aligned} \lambda^- \quad = \quad & \max\ \lambda \\ & \text{s.t} \begin{cases} \mathbf{A}_1\mathbf{m}_1 + \mathbf{A}_2\mathbf{m}_2 + \mathbf{A}_3\mathbf{m}_3 + \lambda q \mathbf{I} = \mathbf{0} \\ \mathbf{B}_1\mathbf{m}_1 + \mathbf{B}_2\mathbf{m}_2 + \mathbf{B}_3\mathbf{m}_3 = \mathbf{0} \\ \boldsymbol{\rho}^k \in \mathscr{L}^k,\ k = 1,\ 2,\ \dots,\ np \end{cases} \end{aligned} \tag{49}$$

where np is the number of yield points. Using the existing Voronoi cell geometry, the yield condition can conveniently be enforced at vertex points within Voronoi cells, as well as at nodes, as indicated in Figure 5.

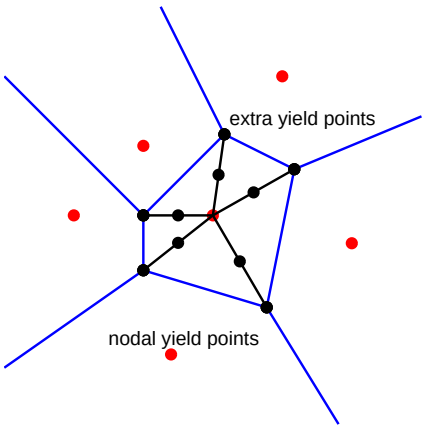

Figure 5. Locations of yield points (at nodes and elsewhere within Voronoi cells)

It should be emphasized that the collapse multiplier λ^- determined using the described procedure is not guaranteed to represent a strict lower-bound on the exact value. This is because the smoothed moment derivative field may not fully satisfy equilibrium conditions everywhere in the domain, and because the yield condition is only enforced at a limited number of points. However, as the numerical discretization becomes increasingly fine one can expect to achieve an increasingly reliable approximation of the actual collapse load multiplier.

5. NUMERICAL EXAMPLES

The performance of the limit analysis procedure described will now be tested by examining a number of benchmark plate and slab problems for which upper and/or lower bound solutions have previously been reported in the literature. For all the examples considered uniform out-of-plane pressure loading was applied and the reference length L was taken as 10 m in the numerical simulations. Problems were setup using MATLAB and the Mosek version 5.0 optimization solver was used to obtain all solutions. Note that for convenience in each case the whole plate or slab problem has been solved, obviating the need to consider symmetry boundary conditions (these can be complicated to treat in the static formulation [31]).

5.1. Reinforced concrete slab examples

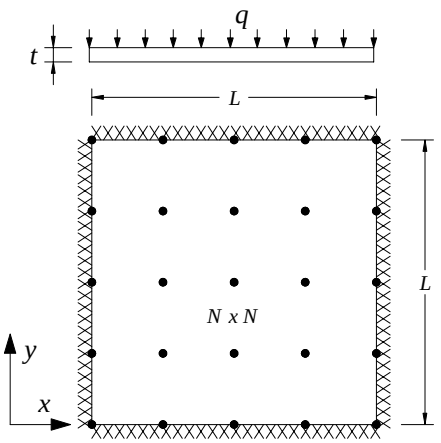

Figure 6. Clamped square slab subject to a uniform pressure load

The first example comprises a clamped square slab, as shown in Figure 6, which has been investigated numerically by Chan [4], Krabbenhoft and Damkilde [31,32] and Krenk et al. [33]. It is assumed that the slab is isotropic with positive and negative yield moments m_p in both directions (constant reinforcement). For this case, the yield criterion (2) may be represented as a square yield locus in the plane of the principal moments [28, 34], and the exact solution has been identified by Fox [35] as

$$\lambda_p = 42.851 \frac{m_p}{qL^2} \tag{50}$$

The problem has been solved using a $N \times N$ nodes uniformly distributed across the whole slab. The solutions obtained with the size of the domain of influence, β, taken as 3 for various values of N are shown in Table I.

Table I. Clamped square slab: variation of collapse load multiplier with level of nodal refinement, N

$N \times N$	10×10	15×15	20×20	30×30	40×40
Collapse multiplier $\lambda^- \left(\frac{m_p}{qL^2}\right)$	42.33	42.67	42.73	42.80	42.83
Errors (%)	1.22	0.42	0.28	0.12	0.05

It can be observed from Table I that close estimates of the exact solution can be obtained even when only a moderate number of nodes are used. For the finest nodal discretization used (40×40 nodes), the solution obtained is very close (within 0.05%) of the exact solution. Furthermore, although it has been pointed out that the procedure cannot be guaranteed to provide strict lower bound solutions, it is clear that all the solutions obtained are below the exact value.

The relationship between the computed collapse load multiplier and the size of the influence domain, governed by the parameter β, are illustrated in Figure 7. It can be observed that, when β is taken to be larger than 3, a higher (i.e. improved) computed load multiplier can sometimes be obtained. However, since the computational cost increases with the size of the influence domain, a reasonable compromise between accuracy and computational cost can be achieved when β is taken as 3, as will be the case for all problems considered henceforth.

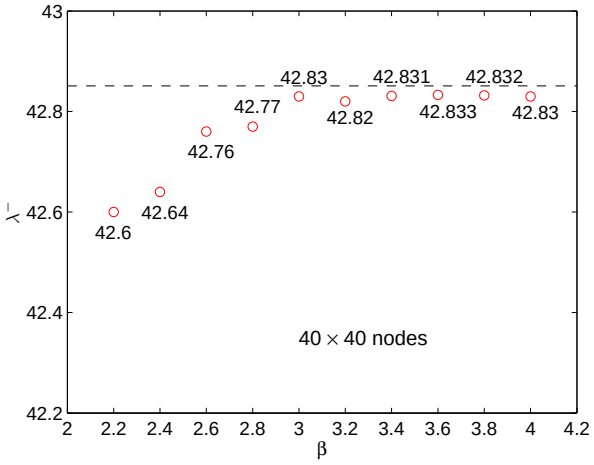

Figure 7. Clamped square slab: normalized collapse load multiplier vs size of the influence domain, β (dotted line represents exact solution of Equation (50))

Compared to results obtained by previous workers, the best solution obtained using the present procedure is significantly higher than that obtained in [33] and [4] (41.78 and 42.32 respectively), and slightly higher than the solution obtained in [32] (42.82), despite the fact that the number of nodes used here is significant smaller than in [32] (40×40 nodes compared

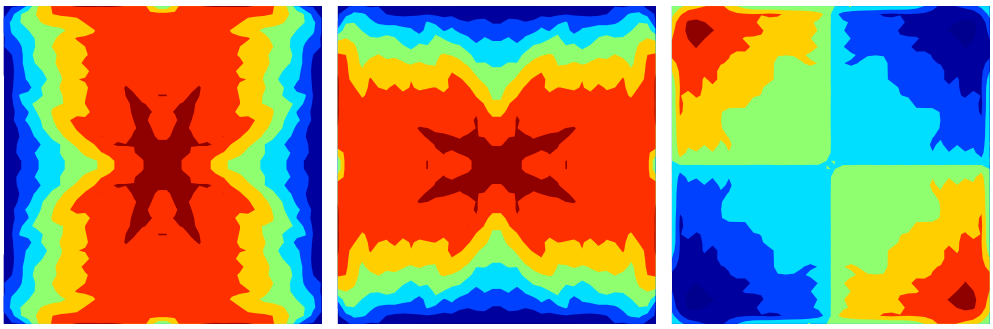

(a) m_{xx}/m_p (b) m_{yy}/m_p (c) m_{xy}/m_p

Figure 8. Clamped square slab: moment distributions

to 101×101 nodes for the whole slab). The moment distributions at collapse are shown in Figure 8.

A simply supported isotropic square slab will be considered next. For this case the exact collapse load multiplier was given in [8] as $\lambda_p = 24\frac{m_p}{qL^2}$. When 20×20 nodes were used to model the slab, the corresponding normalized collapse multiplier was found to be 23.996, which is clearly in excellent agreement with the exact solution.

The method will next be applied to a clamped isotropic circular slab subjected to a uniform pressure loading. The exact collapse multiplier was given in [8] as $\lambda_p = 12\frac{m_p}{qR^2}$, where R is the slab radius. The problem was solved using an irregular layout of nodes comprising 49 nodes laid out over the slab, as shown on Figure 9. A normalized solution of 11.89 was obtained, which is just 0.9% lower than the exact collapse multiplier.

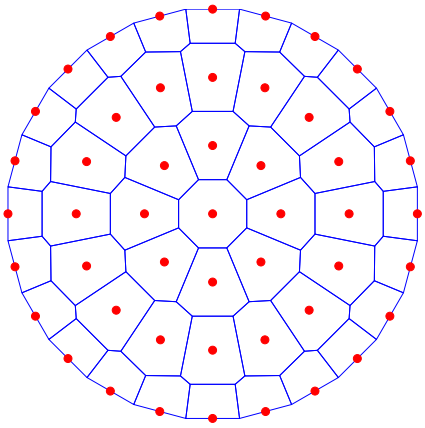

Figure 9. Clamped circular slab: nodal discretization and Voronoi cells

5.2. Metal plate examples

Square steel plates with either clamped or simply supports on all edges will now be considered; these have also been investigated by Hodge and Belytschko [1], Andersen et al. [36], Capsoni and Corradi [2], and more recently by Le et al. [9]. The problems were solved using $N \times N$ nodes uniformly distributed across the whole plate and in all numerical simulations the plate thickness was taken as $t = 0.1$ m. The solutions and CPU times are shown in Table II for various levels of nodal refinement.

Table II. Clamped & simply supported square plates: results for different level of nodal refinement, N

	clamped		simply supported	
$N \times N$	$\lambda^-(\frac{m_p}{qL^2})$	CPU time (s)†	$\lambda^-(\frac{m_p}{qL^2})$	CPU time (s)†
14×14	43.2467	30	24.8554	42
18×18	43.5364	107	24.9175	97
22×22	43.6961	304	24.9462	226
30×30	43.8562	952	24.9766	882

†Time taken to solve on a 2.8GHz Pentium 4 PC running Microsoft XP (Mosek time only)

Table III compares normalized solutions obtained using the present method with upper and lower bound solutions that have previously been reported in the literature. It can be observed that the solutions obtained using the present method are in good agreement with previous results. For both clamped and simply supported plate problems, the solutions obtained here are higher than the best lower-bounds obtained in [1] (2.33% in the case of the clamped plate and 0.48% in the case of the simply supported plate). Together with [9], this indicates that numerical limit analysis procedures which use the EFG method are capable of producing good results. Note that in the case of the simply supported square plate, the mean value of the lower-bound obtained here and the upper-bound obtained in [9] is 24.995, which is evidently in excellent agreement with the solution obtained by Andersen et al. [36]. Moment distributions at collapse for these plates are shown in Figures 10 and 11.

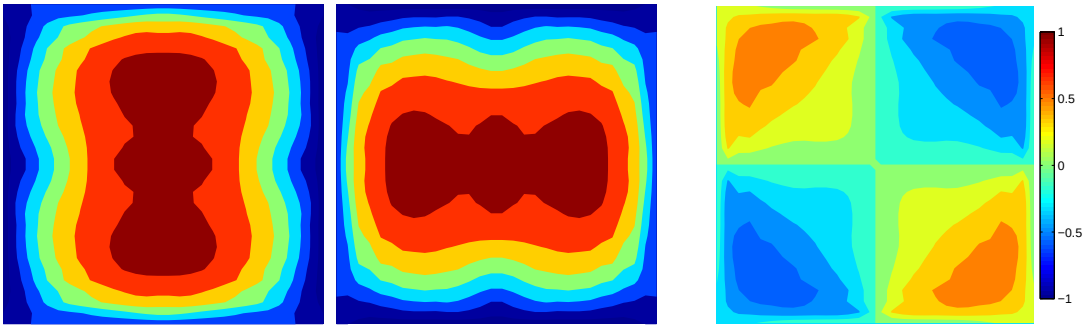

(a) m_{xx}/m_p (b) m_{yy}/m_p (c) m_{xy}/m_p

Figure 10. Clamped square plate: moment distributions

Table III. Clamped & simply supported square plates: comparison with literature results

Authors	clamped		simply supported	
	lower-bound (LB)	upper-bound (UB)	lower-bound (LB)	upper-bound UB)
Present method	43.86*	–	24.98*	–
Le et al. [9] (EFG method)	–	45.07*	–	25.01*
Hodge and Belytschko [1]	42.86	49.25	24.86	26.54
Lubliner [3]	–	52.01	23.81	27.71
Capsoni and Corradi [2]	–	45.29	–	25.02
Andersen et al. [36]	44.13‡		25.00‡	

* methods produce approximate rather than rigorous lower or upper bound solutions

‡ mixed elements were used

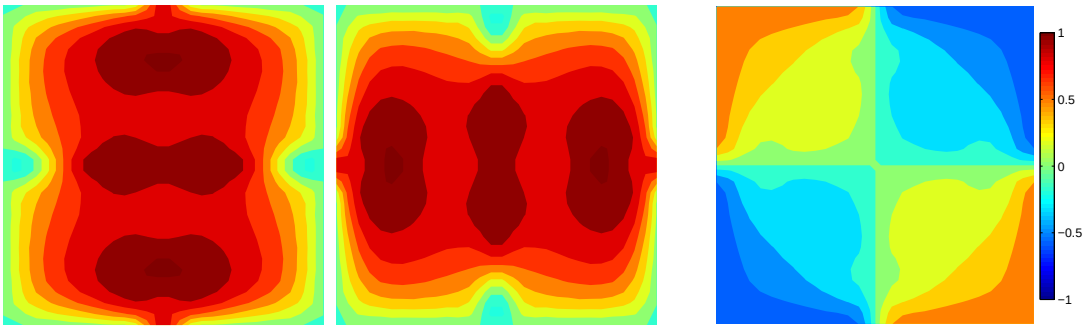

(a) m_{xx}/m_p (b) m_{yy}/m_p (c) m_{xy}/m_p

Figure 11. Simply supported square plate: moment distributions

Rectangular plates (dimensions $a \times b$) with different boundary conditions will now be considered. All problems here were solved using 60×30 nodes with $a = 2b = 10$ m. In case of the plate with 3 clamped boundaries and 1 free edge, note that the free edge has length b. Collapse load multipliers are shown in Table IV. It can be observed from the table that the gaps between the (approximate) lower-bounds found in this paper and (approximate) upper-bounds in [9] are narrow, particularly for the case of a rectangular plate with simply supported boundaries.

Table IV. Rectangular plates: collapse loads multipliers with various boundary conditions ($\frac{m_p}{qab}$)

Models	clamped	simply supported	3 clamped, 1 free
Present results	53.43	29.85	43.11
Le et al. [9]	54.61	29.88	43.86
Capsoni et at. [2](UB)	–	29.88	–

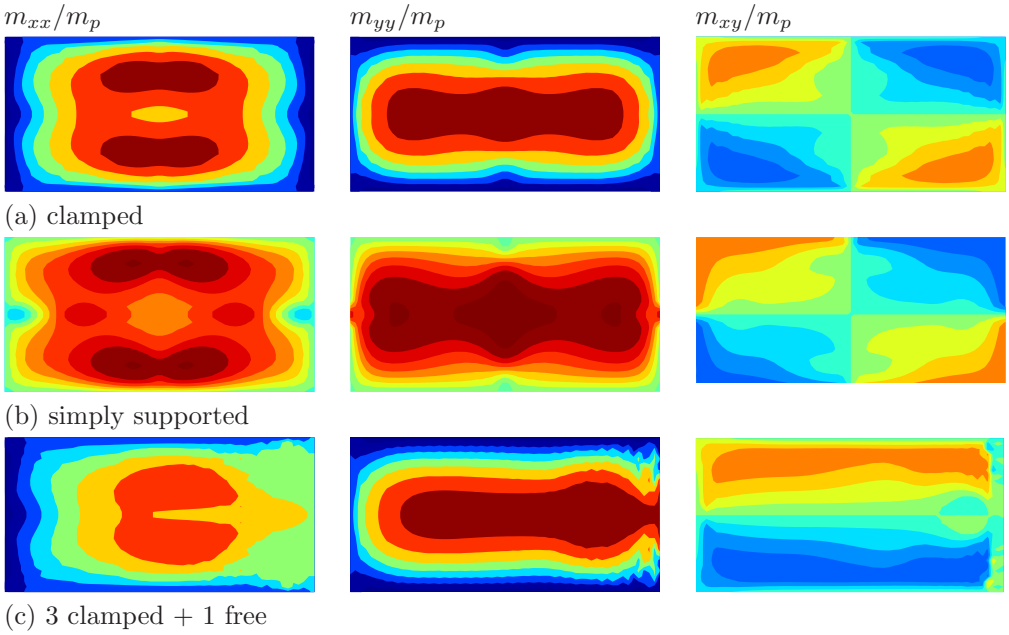

Figure 12. : Rectangular plates: moment distributions

Moment distributions at collapse are shown in Figure 12. In plates containing free boundaries it can be observed that the moments oscillate slightly close to a free edge, as shown in Figure 12c. This may be explained by the fact that average values of the shear forces were used to enforce the shear boundary condition. However, if the shear forces are computed using the actual values of the moment derivatives (rather than the smoothed values given in Equations (28) and (29)), larger oscillations result.

6. CONCLUSIONS

An Element-Free Galerkin (EFG) based equilibrium limit analysis formulation has been proposed. This uses a moving least squares approximation of the moment field, which means that the resulting field is smooth over the entire problem domain. The collocation method is used in combination with the stabilized conforming nodal integration (SCNI) scheme to ensure that equilibrium needs only to be enforced at nodes. The Nielsen and von Mises yield criteria are formulated as second-order cones so that the underlying limit analysis problem becomes a standard second-order cone programming problem, which can be solved efficiently using primal-dual interior point solvers. Although the procedure cannot be guaranteed to produce strict lower bound solutions, for the plate and slab problems investigated solutions were in practice always lower than known exact solutions, and higher than (improved cf.) existing lower bound numerical solutions in the literature.

ACKNOWLEDGEMENTS

This research has been sponsored by the Ho Chi Minh City Government (300 Masters & Doctors Project) and the University of Sheffield. Matthew Gilbert also acknowledges the support of EPSRC under grant reference GR/S53329/01.

REFERENCES

1. Ph. G. Jr. Hodge and T. Belytschko. Numerical Methods for the Limit Analysis of Plates. *Trans. ASME, Journal of Applied Mechanics*, 35:796–802, 1968.
2. A. Capsoni and L. Corradi. Limit analysis of plates - a finite element formulation. *Structural Engineering and Mechanics*, 8:325–341, 1999.
3. J. Lubliner. *Plasticity theory.* Macmillan, New York, 1990.
4. H. S. Y. Chan. The collapse load of reinforeced concrete plates. *International Journal for Numerical Methods in Engineering*, 5:57–64, 1972.
5. E. Anderheggen and H. Knopfel. Finite element limit analysis using linear programming. *International Journal of Solids and Structures*, 8:1413–1431, 1972.
6. E. Faccioli and E. Vitiello. A finite element, linear programming methods for the limit analysis of thin plates. *International Journal for Numerical Methods in Engineering*, 5:311–325, 1973.
7. J. Munro and A. Da Fonseca. Yield line method by finite elements and linear programming. *The Structural Engineer*, 56:37–44, 1978.
8. M. A. Save, C. E Massonnet, and G. de Saxce. *Plastic analysis and design of plates, shells and disks.* North-Holland Series in Applied Mathematics and Mechanics, 43, Elsevier, 1997.
9. C. V. Le, M. Gilbert, and H. Askes. Limit analysis of plates using the EFG method and second-order cone programming. *International Journal for Numerical Methods in Engineering*, 78:1532–1552, 2009.
10. S. Chen, Y. Liu, and Z. Cen. Lower-bound limit analysis by using the EFG method and non-linear programming. *International Journal for Numerical Methods in Engineering*, 74:391–415, 2008.
11. J. S. Chen, C. T. Wu, S. Yoon, and Y. You. A stabilized conforming nodal integration for Galerkin mesh-free methods. *International Journal for Numerical Methods in Engineering*, 50:435–466, 2001.
12. K. Y. Sze, J. S. Chen, N. Sheng, and X. H. Liu. Stabilized conforming nodal integration: exactness and variational justification. *Finite Elements in Analysis and Design*, 41:147–171, 2004.
13. D. Wang and J. S. Chen. Locking-free stabilized conforming nodal integration for meshfree Mindlin-Reissner plate formulation. *Computer Methods in Applied Mechanics and Engineering*, 193:1065–1083, 2004.
14. J. W. Yoo, B. Moran, and J. S. Chen. Stabilized conforming nodal integration in the natural-element method. *International Journal for Numerical Methods in Engineering*, 60:861–890, 2004.
15. Mosek. *The MOSEK optimization toolbox for MATLAB manual. http://www.mosek.com.* Mosek ApS, version 5.0 edition, 2008.
16. M. P. Nielsen. *Limit analysis of reinforced concrete slabs.* Acta-Polytechnica. Danmark: Kobenhavn, 1964.
17. R. Wolfensberger. *Traglast und optimale Bemessung von Platten.* Zurich, Schweiz: ETH, 1964.
18. M. P. Nielsen. *Limit analysis and concrete plasticity.* CRC Press, 1998.
19. T. Belytschko, Y. Y. Lu, and L. Gu. Element-Free Galerkin methods. *International Journal for Numerical Methods in Engineering*, 37:229–256, 1994.
20. O. C. Zienkiwicz and R. L Taylor. *The Finite Element Method, Volume 1: The Basis.* Butterworth-Heinemann; 5 edition, 2000.
21. G. R. Liu and Y. T. Gu. *An Introduction to Meshfree Methods and Their Programming.* Springer, 2005.
22. Y. Chen, J. Lee, and A. Eskandarian. *Meshless Methods in Solid Mechanics.* Springer, 2006.
23. B. Fraeijs de Veubeke. Displacement and equilibrium models in the finite element method. *International Journal for Numerical Methods in Engineering, Reprinted*, 52:287–342, 2001.
24. B. Fraeijs de Veubeke and O. C. Zienkiewicz. Strain-energy bounds in finite element analysis by slab analogy. *Journal of Strain Analysis*, 2:265–271, 1967.
25. M. Duflot and H. Nguyen-Dang. Dual analysis by a meshless method. *Communications in Numerical Methods in Engineering*, 18:621–631, 2002.
26. J. S. Chen, C. T. Wu, and T. Belytschko. Regularization of material instabilities by meshfree approximations with intrinsic length scales. *International Journal for Numerical Methods in Engineering*, 47:1303–1322, 2000.
27. T. Zhu and S. N. Atluri. A modified collocation method and a penalty formulation for enforcing the essential boundary conditions in the element free Galerkin method. *Computational Mechanics*, 21:211–222, 1998.

28. K. Krabbenhoft, A. V. Lyamin, and S. W. Sloan. Formulation and solution of some plasticity problems as conic programs. *International Journal of Solids and Structures*, 44:1533–1549, 2007.
29. H. Ciria, J. Peraire, and J. Bonet. Mesh adaptive computation of upper and lower bounds in limit analysis. *International Journal for Numerical Methods in Engineering*, 75:899–944, 2008.
30. A. Makrodimopoulos and C. M. Martin. Upper bound limit analysis using simplex strain elements and second-order cone programming. *International Journal for Numerical and Analytical Methods in Geomechanics*, 31:835–865, 2006.
31. K. Krabbenhoft and L. Damkilde. Lower bound limit analysis of slabs with nonlinear yield criteria. *Computers and Structures*, 80:2043–2057, 2002.
32. K. Krabbenhoft and L. Damkilde. A general nonlinear optimization algorithm for lower bound limit analysis. *International Journal for Numerical Methods in Engineering*, 56:165–184, 2003.
33. S. Krenk, L. Damkilde, and O. Hoyer. Limit analysis and optimal design of plates with equilibrium elements. *Journal of Engineering Mechanics*, 120:1237–1254, 1994.
34. M. W. Braestrup. Yield line theory and concrete plasticity. *Magazine of Concrete Research*, 60:549–553, 2008.
35. E. N. Fox. Limit analysis for plates: The exact solution for a clamped square plate of isotropic homogeneous material obeying the square yield criterion and loaded by uniform pressure. *Philosophical Transactions of the Royal Society of London, Series A*, 277:121–155, 1974.
36. K. D. Andersen, E. Christiansen, and M. L. Overton. Computing limit loads by minimizing a sum of norms. *SIAM Journal on Scientific Computing*, 19:1046–1062, 1998.